Lumrey, R., & Rajender, S. (1970) *Biopolymers 9*, 1125-1227.
Nishimura, S., Mashimo, T., Hiraki, K., Hamanaka, T., Kito, Y., & Yoshiya, I. (1985) *Biochim. Biophys. Acta 818*, 421-424.
Oesterhelt, D., Meentzen, M., & Schuhmann, L. (1973) *Eur. J. Biochem. 40*, 453-463.
Pande, J., Callender, R. H., & Ebrey, T. G. (1981) *Proc. Natl. Acad. Sci. U.S.A. 78*, 7379-7382.
Pande, A., Callender, R., Ebrey, T., & Tsuda, M. (1984) *Biophys. J. 45*, 573-576.
Pettei, M., Yudd, A. P., Nakanishi, K., Henselman, R., & Stoeckenius, W. (1977) *Biochemistry 16*, 1955-1958.
Rothschild, K. J. (1988) *Photochem. Photobiol. 47*, 883-887.
Schreckenbach, T., Walckhoff, B., & Oesterhelt, D. (1977) *Eur. J. Biochem. 6*, 499-511.
Schreckenbach, T., Walckhoff, B., & Oesterhelt, D. (1978) *Biochemistry 17*, 5353-5359.
Spudich, J., McCaine, D. A., Nakanishi, K., Okabe, M., Shimizu, N., Rodman, H., Honig, B., & Bogomolni, R. (1986) *Biophys. J. 49*, 479-483.
Tsygannik, I. N., & Baldwin, J. M. (1987) *Eur. Biophys. J. 14*, 263-272.
Unwin, P. N. T., & Henderson, R. (1975) *J. Mol. Biol. 94*, 425-440.

Analysis of the Relative Contributions of the Nuclear Overhauser Interproton Distance Restraints and the Empirical Energy Function in the Calculation of Oligonucleotide Structures Using Restrained Molecular Dynamics†

Angela M. Gronenborn* and G. Marius Clore*
Laboratory of Chemical Physics, Building 2, National Institute of Diabetes and Digestive and Kidney Diseases, National Institutes of Health, Bethesda, Maryland 20892
Received February 21, 1989; Revised Manuscript Received April 5, 1989

ABSTRACT: The relative contributions of the interproton distance restraints derived from nuclear Overhauser enhancement measurements and of the empirical energy function in the determination of oligonucleotide structures by restrained molecular dynamics are investigated. The calculations are based on 102 intraresidue and 126 interresidue interproton distance restraints derived from short mixing time two-dimensional nuclear Overhauser enhancement data on the dodecamer 5'd(CGCGPATTCGCG)$_2$ [Clore, G. M., Oschkinat, H., McLaughlin, L. W., Benseler, F., Scalfi Happ, C., Happ, E., & Gronenborn, A. M. (1988) *Biochemistry 27*, 4185-4197]. Eight interproton distance restraint lists were made up with errors ranging from $-0.1/+0.2$ to $-1.2/+1.3$ Å for $r < 2.5$ Å and from $-0.2/+0.3$ to $-1.3/+1.4$ Å for $r \geq 2.5$ Å. These restraints were incorporated into the total energy function of the system in the form of square-well potentials with force constants set sufficiently high to ensure that the deviations between calculated distances and experimental restraints were very small (average interproton distance rms deviation of less than 0.06 Å). For each data set, six calculations were carried out, three starting from classical A-DNA and three from classical B-DNA. The results show that structural changes occurring during the course of restrained molecular dynamics and the degree of structural convergence are determined by the interproton distance restraints. All the structures display similar small deviations from idealized geometry and have the same values for the nonbonding energy terms comprising van der Waals, electrostatic, and hydrogen-bonding components. Thus, the function of the empirical energy function is to maintain near perfect stereochemistry and nonbonded interactions. Local structural variations can be determined up to error limits of $-0.2/+0.3$ Å for $r < 2.5$ Å and $-0.3/+0.4$ Å for $r \geq 2.5$ Å. Up to error limits of $-0.4/+0.5$ Å for $r < 2.5$ Å and $-0.5/+0.6$ Å for $r \geq 2.5$ Å local structural variations are still discernible, although the spread of the structures becomes appreciably larger. For larger error limits local structural variations cannot be assessed at all.

Over the last few years considerable success has been achieved in determining three-dimensional structures of macromolecules in solution by nuclear magnetic resonance (NMR)[1] spectroscopy on the basis of NOE-derived interproton distance restraints [see Wüthrich (1986, 1989) and Clore and Gronenborn (1987, 1989) for reviews]. While the application of this methodology in the case of proteins has now been widely accepted, there has been some dispute regarding its application to oligonucleotides. This has arisen in part because the distance restraints for oligonucleotides are limited to adjacent base pairs so that, unlike in proteins, there are no tertiary NOE restraints to position non nearest neighbors with respect to each other. There have been essentially two schools of thought. The first has made use of metric matrix distance geometry calculations and has asserted that as the algorithm uses exclusively distance information the resulting structures are determined solely from the experimental distance restraints (Hare & Reid, 1986; Hare et al., 1986a,b; Reid, 1987; Patel et al., 1987; Nerdal et al., 1988; Pardi et al., 1988). The second

† This work was supported by the Intramural AIDS Anti-Viral Targeted Program of the Office of the Director of the National Institutes of Health.

[1] Abbreviations: NMR, nuclear magnetic resonance; NOE, nuclear Overhauser effect; RD, restrained dynamics; rms, root mean square.

has made use of restrained molecular dynamics in which an effective potential representing the experimentally derived interproton distances is added to the empirical energy function describing bonded and nonbonded interactions (Nilsson et al., 1986; Nilges et al., 1987a,b; Behling et al., 1987; Clore et al., 1988; Scalfi Happ et al., 1988). The rationale behind this latter approach is to ensure that the resulting structures not only satisfy the experimental distance restraints but also display near perfect stereochemistry. Controversy, however, has centered in particular on the relative contributions of the experimental restraints and the empirical energy function in restrained molecular dynamics, with the distance geometry school claiming that "it is not possible to evaluate to what extent the precision and accuracy of the structures are affected by the distance constraints and to what extent they are affected by energy potentials" (Pardi et al., 1988). This same argument, however, is equally applicable to the distance geometry calculations as they also require the use of an empirical energy function, even though this may not be transparent at first glance. Specifically, distance restraints are required to maintain correct covalent geometry (i.e., bonds, angles, and planes) and to ensure appropriate van der Waals contacts (i.e., lower distance limits between atom pairs set to the sum of the van der Waals radii). In the absence, for example, of a van der Waals repulsion term, the interproton distance restraints cannot define a structure.

To address in a systematic manner the problem stated above with respect to the restrained dynamics approach, we have carried out a series of restrained molecular dynamics calculations using different error limits for experimental distance restraints. The results show that the driving force for the structural changes occurring during the course of the calculations arises from the interproton distance restraints, while the empirical energy function serves to maintain good covalent geometry and nonbonded contacts. Thus, the nonbonding energies, as well as the deviations from idealized covalent geometry, have the same values for all the structures calculated, independent of the error limits on the interproton distance restraints.

Methods

All energy minimization and restrained molecular dynamics calculations were carried out with a version of the program X-PLOR (Brünger, 1988) adapted for the Star ST-50 array processor (B. R. Brooks, unpublished data). X-PLOR was derived originally from the molecular dynamics program CHARMM (Brooks et al., 1983) and has been especially adapted for restrained molecular dynamics calculations for structure determination on the basis of NMR (Clore et al., 1985, 1986a; Brünger et al., 1986; Nilges et al., 1988) and X-ray (Brünger et al., 1987) data. The all-hydrogen empirical energy function used was that developed by Nilsson and Karplus (1985) for nucleic acids. With respect to the electrostatic component of the empirical energy function, the effect of solvent was approximated by a $1/r$ screening function (Gelin & Karplus, 1977; Brooks et al., 1983) and by reducing the net charge on the phosphate group to −0.32 e (Tidor et al., 1982). The nonbonded interactions were switched off between 9.5 and 10.5 Å by using a cubic switching function, and pairs up to 11.5 Å were included in the nonbonded list. Integration of Newton's equations of motion was carried out with a Verlet (1967) integration algorithm with initial velocities assigned from a Maxwellian distribution at 400 K. The temperature was maintained constant by rescaling the velocities of the atoms every 100 fs. The time step of the integrator was 1 fs, and the nonbonded interaction lists were updated every 20 fs. Bond lengths involving hydrogen atoms were kept fixed with the SHAKE algorithm (Ryckaert et al., 1977).

Table I: Error Limits for the Interproton Distance Restraints Used To Calculate the Different Restrained Dynamics Structural Sets

structure set	data set	error limits for distance restraints (Å)	
		$r < 2.5$ Å	$r \geq 2.5$ Å
⟨a⟩	a	−0.1/+0.2	−0.2/+0.3
⟨b⟩	b	−0.2/+0.3	−0.3/+0.4
⟨c⟩	c	−0.3/+0.4	−0.4/+0.5
⟨d⟩	d	−0.4/+0.5	−0.5/+0.6
⟨e⟩	e	−0.6/+0.7	−0.7/+0.8
⟨f⟩	f	−0.8/+0.9	−0.8/+1.0
⟨g⟩	g	−1.2/+1.3	−1.3/+1.4

Calculational Strategy

The calculations were carried out by using experimental restraints for the dodecamer 5′d(CGCGPATTCGCG)$_2$ that we had determined previously from short mixing time NOESY data (Clore et al., 1988). These comprised a total of 258 restraints made up of 102 intraresidue and 126 interresidue interproton distance restraints [see Table II of Clore et al. (1988)] and 30 base-pairing restraints [see Table IV of Clore et al. (1988)]. From these data, eight interproton distance restraint lists were made up with error limits ranging from −0.1/+0.2 to −1.3/+1.4 Å. These are summarized in Table I. The error limit for the hydrogen bond base-pairing restraints was held constant throughout at ±0.1 Å.

The strategy used in the restrained molecular dynamics calculations (Clore et al., 1985, 1986a; Kaptein et al., 1985; Nilsson et al., 1986) seeks to minimize the total energy of the system by solving Newton's equations of motion. By incorporating kinetic energy into the system, energy barriers along the path toward the global minimum region can be efficiently overcome (cf. simulated annealing from a random array of atoms; Nilges et al., 1988). The total energy is given by

$$E_{tot} = E_{empirical} + E_{NMR} \quad (1)$$

$E_{empirical}$ is given by the sum of covalent ($E_{covalent}$) and nonbonding ($E_{nonbonding}$) terms

$$E_{covalent} = E_{bond} + E_{angle} + E_{improper} \quad (2)$$

where $E_{improper}$ serves to maintain planarity and chirality, and

$$E_{nonbonding} = E_{vdW} + E_{electrostatic} + E_{hbond} \quad (3)$$

E_{NMR} is composed of a NOE (E_{NOE}) and a dihedral (E_{tor}) term. In the present calculations the potential form used for E_{NOE} is a square-well potential (Clore et al., 1986b) given by

$$\begin{aligned} E_{NOE} &= k_{NOE}(r_{ij} - r_{ij}^{u})^2 && \text{if } r_{ij} > r_{ij}^{u} \\ &= 0 && \text{if } r_{ij}^{l} \leq r_{ij} \leq r_{ij}^{u} \\ &= k_{NOE}(r_{ij} - r_{ij}^{l})^2 && \text{if } r_{ij} < r_{ij}^{l} \end{aligned} \quad (4)$$

where r_{ij} is the calculated distance, r_{ij}^{u} and r_{ij}^{l} are the upper and lower limits of the experimental restraints, and k_{NOE} is the NOE restraint force constant. Providing k_{NOE} is large, this potential form ensures that the calculated distances lie within the specified error limits. This permits a clear-cut analysis of the results in terms of the errors in the interproton distances, which would not have been possible in a transparent fashion with the skewed biharmonic potential (Nilsson et al., 1986) employed in the previous work (Clore et al., 1988) since in that case the error is reflected only in the steepness of the walls of the potential. This is evident from the diagrammatic representation of these two potential forms shown in Figure 1.

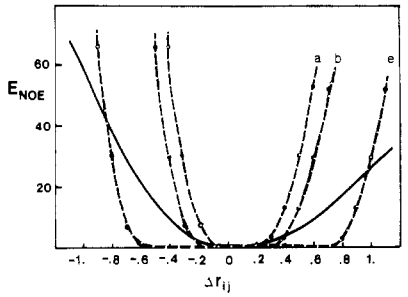

FIGURE 1: Diagrammatic representation of the square-well NOE potential (---) for different distance errors and of the skewed biharmonic potential used by Clore et al. (1988). The square-well potentials are calculated with a force constant of 200 kcal mol^{-1} Å^{-2} and error limits of (a) −0.1/+0.2 Å, (b) −0.2/+0.3 Å, and (e) −0.6/+0.7 Å. The force constants for $r_{calc} < r_0$ and for $r_{calc} > r_0$ are 59.6 and 26.5 kcal mol^{-1} Å^{-2}, respectively, in the case of the skewed biharmonic potential; these are the values taken by Clore et al. (1988) to correspond to error estimates of −0.2 and +0.3 Å, respectively. The units of E_{NOE} are kcal mol^{-1} and of Δr_{ij} are Å.

The dihedral term E_{tor} is also represented by a square-well potential with a force constant k_{tor} of 50 kcal mol^{-1} rad^{-2}

$$\begin{aligned} E_{tor} &= k_{tor}(\varphi_i - \varphi_i^u)^2 && \text{if } \varphi_i > \varphi_i^u \\ &= 0 && \text{if } \varphi_i^l \le \varphi_i \le \varphi_i^u \\ &= k_{tor}(\varphi_i - \varphi_i^l)^2 && \text{if } \varphi_i < \varphi_i^l \end{aligned} \quad (5)$$

where φ_i^u and φ_i^l and the upper and lower limits of the torsion angle restraint i and φ_i is the calculated value. The δ torsion angles were restrained to lie in the range 140 ± 30° on the basis of the coupling constant data which indicated that they had to have values ≥110° (Clore et al., 1988). The α, β, γ, ϵ, and ζ torsion angles were restricted to broad ranges of 180 ± 50°, −85 ± 50°, −70 ± 50°, 180 ± 50°, and 60 ± 35°. These torsion angle restraints describe ranges characteristic of right-handed DNA (both A and B type) and were used to avoid problems associated with local mirror images commonly found in structures determined from NMR distance restraints. It should be noted that examination of the values for these torsion angles in both fiber diffraction structures and single-crystal structures of all right-handed DNAs indicates that these lie well within the ranges of the above torsion angle restraints. In addition, the torsion angles for the starting structures as well as the converged restrained dynamics structures lie within these ranges and have an E_{tor} value of 0.

The protocol of restrained dynamics used was as follows: 4 ps at 400 K during which time k_{NOE} was increased from 0.477 to a maximum value of 200 kcal mol^{-1} Å^{-2} by multiplying its value by $10^{0.2}$ every 0.1 ps, followed by 10 ps of restrained dynamics at 300 K. The coordinates of the last 6 ps were then averaged and subjected to 400 cycles of restrained energy minimization to generate the final restrained dynamics structures. The final value of 200 kcal mol^{-1} Å^{-2} for k_{NOE} ensures that the rms deviation between the calculated distances and the target upper or lower bounds is very small (<0.06 Å). To put the value of k_{NOE} in perspective, we note that the values for the bond force constants lie between 200 and 600 kcal mol^{-1} Å^{-2}.

Calculations were carried out by starting from classical A-DNA and classical B-DNA. The atomic rms difference between these two starting structures is 6.24 Å. Three restrained dynamics runs were carried out for each starting structure by using different random number seeds for the assignments of the initial velocities. Thus, for each restraint data set six restrained dynamics (RD) structures were calculated. The notation of the restrained dynamics structures used is as follows: $\langle x \rangle$ are the six RD structures calculated by using data set x, and $\bar{x}$ is the mean structure obtained by averaging the coordinates of the individual RD structures best fitted to each other.

Table II: Nonbonding Energies of the Restrained Dynamics Structures and the Energy-Minimized Classical A- and B-DNA Structures

structure set	energies (kcal mol^{-1}) van der Waals	electrostatic	H-bond	rms deviation for H-bond restraints[a] (Å)
⟨a⟩	−386 ± 2	−481 ± 9	−84 ± 15	0.040 ± 0.004
⟨b⟩	−389 ± 1	−492 ± 8	−77 ± 20	0.039 ± 0.003
⟨c⟩	−389 ± 1	−498 ± 6	−78 ± 21	0.042 ± 0.006
⟨d⟩	−388 ± 3	−498 ± 9	−77 ± 19	0.045 ± 0.004
⟨e⟩	−388 ± 3	−500 ± 12	−84 ± 15	0.047 ± 0.002
⟨f⟩	−389 ± 4	−502 ± 13	−81 ± 12	0.045 ± 0.004
⟨g⟩	−395 ± 12	−498 ± 10	−81 ± 21	0.048 ± 0.003
$(A\text{-}DNA)_m$[b]	−387	−507	−75	0.093
$(B\text{-}DNA)_m$[b]	−387	−501	−93	0.097

[a] There are 30 hydrogen bonding base pairing restraints with error limits of ±0.1 Å for all calculations. These are as follows: for A–T base pairs $r_{A(N6)\text{-}T(O4)}$ = 2.95 ± 0.1 Å and $r_{A(N1)\text{-}T(N3)}$ = 2.82 ± 0.1 Å; for P–T base pairs $r_{P(N1)\text{-}C(N3)}$ = 2.82 ± 0.1 Å; for G–C base pairs $r_{G(O6)\text{-}C(N4)}$ = 2.91 ± 0.1 Å, $r_{G(N1)\text{-}C(N3)}$ = 2.95 ± 0.1 Å, and $r_{G(N2)\text{-}C(O2)}$ = 2.86 ± 0.1 Å. These values were taken from X-ray analyses of ApU (Seeman et al., 1976) and GpC (Rosenberg et al., 1976). [b] $(A\text{-}DNA)_m$ and $(B\text{-}DNA)_m$ are the structures obtained by subjecting classical A- and B-DNA to 2500 cycles of Powell energy minimization in the absence of interproton distance restraints. This procedure results in atomic rms shifts of less than 0.5 Å. (Note that the hydrogen-bonding distance restraints are not used in these calculations and the base-pairing hydrogen bonding is represented solely by the hydrogen-bonding potential of the empirical energy function.)

Table III: Deviations from Idealized Geometry for the Restrained Dynamics Structures and the Energy-Minimized Classical A- and B-DNA Structures

structure set	deviations from idealized geometry bonds (Å)	angles (deg)	impropers[a] (deg)
⟨a⟩	0.007 ± 0	3.193 ± 0.029	0.265 ± 0.005
⟨b⟩	0.007 ± 0	3.150 ± 0.018	0.230 ± 0.006
⟨c⟩	0.007 ± 0	3.128 ± 0.024	0.195 ± 0.020
⟨d⟩	0.007 ± 0	3.133 ± 0.022	0.183 ± 0.016
⟨e⟩	0.007 ± 0	3.142 ± 0.010	0.166 ± 0.013
⟨f⟩	0.007 ± 0.0004	3.182 ± 0.022	0.163 ± 0.015
⟨g⟩	0.007 ± 0	3.192 ± 0.055	0.170 ± 0.027
$(A\text{-}DNA)_m$[b]	0.006	3.357	0.168
$(B\text{-}DNA)_m$[b]	0.006	3.193	0.150

[a] The improter torsion terms serve to maintain planarity and chirality. [b] $(A\text{-}DNA)_m$ and $(B\text{-}DNA)_m$ are the structures obtained by subjecting classical A- and B-DNA to 2500 cycles of Powell energy minimization in the absence of interproton distance restraints. The procedure results in atomic rms shifts of less than 0.5 Å.

Results and Discussion

The results of the calculations, which are summarized in Tables II–IV and Figures 2–4, permit the following conclusions to be made.

The values of the empirical energy terms are essentially *identical* for all eight RD structure sets. In addition, they are comparable to those of classical A- and B-DNA subjected to energy minimization in the absence of interproton distance restraints, a procedure that results in atomic rms shifts of less than 0.5 Å. All the structures exhibit very small deviations from idealized geometry (Table II) and have very good nonbonded contacts as evidenced by large negative values for the Lennard-Jones van der Waals energy (Table III). Thus, the empirical energy function does *not* provide the driving force for the structural changes that occur during the course of the calculations. It does, however, ensure near perfect stereo-

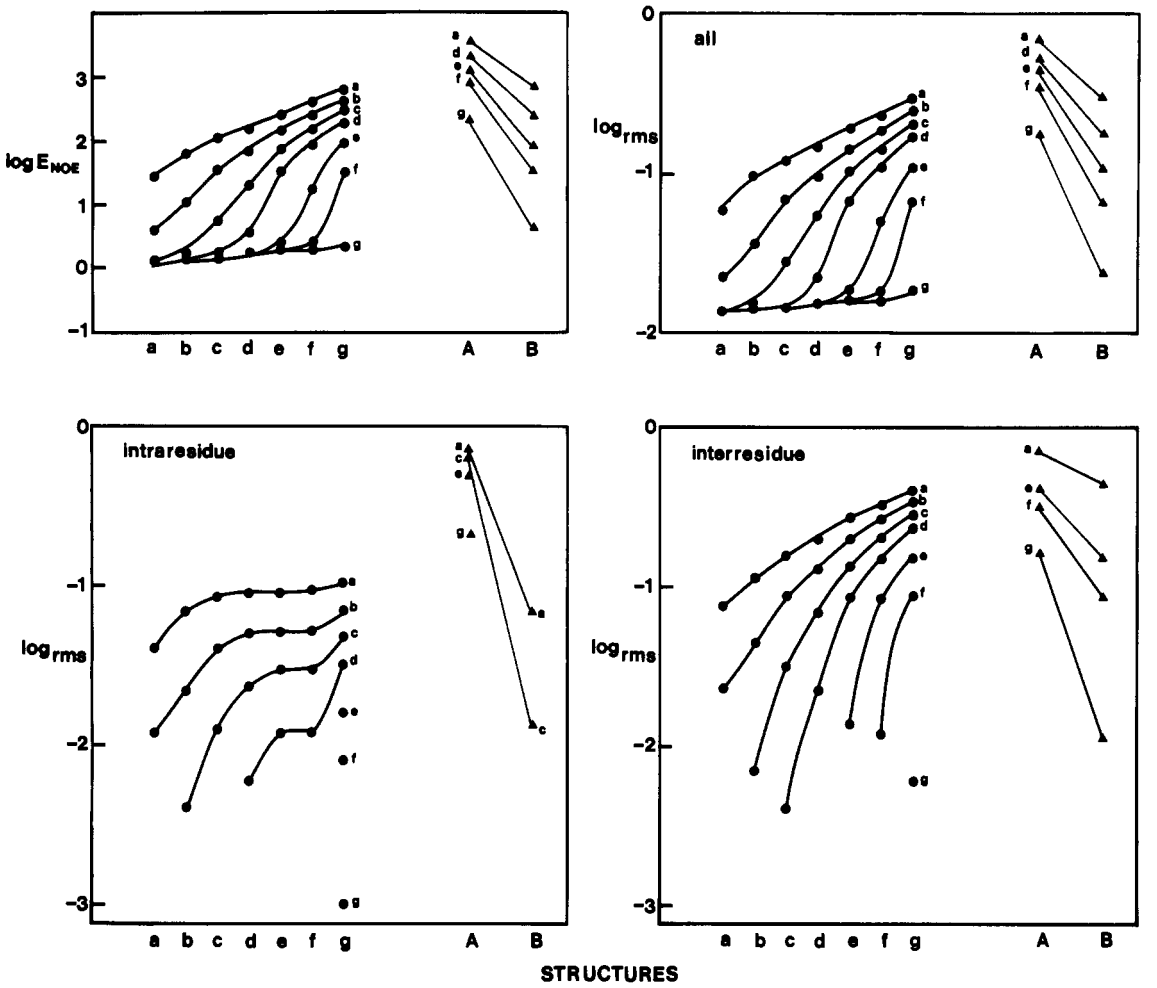

FIGURE 2: Plot of E_{NOE} and interproton distance deviations for the eight RD structure sets ($\langle a\rangle$–$\langle g\rangle$) and classical A- and B-DNA versus the eight restraint data sets (a–g). E_{NOE} (in kcal mol^{-1}) and the interproton distance deviations (in Å) are plotted on a logarithmic scale. Interproton distance deviations are shown for all interproton distance restraints as well as for the intraresidue and the interresidue interproton distance restraints individually. The error limits for the different restraint data sets are given in Table I.

Table IV: Atomic rms Deviations

	atomic rms differences (Å)				
structure	vs A-DNA[a]	vs B-DNA[a]	vs $\bar{a}$[b]	vs $\bar{b}$[b]	vs each other
B-DNA	6.24				
$\bar{a}$	5.43	1.75			
$\bar{b}$	5.55	1.60	0.38		
$\langle a\rangle$	5.45 ± 0.20	1.82 ± 0.13	0.47 ± 0.18	0.60 ± 0.19	0.74 ± 0.23
$\langle b\rangle$	5.57 ± 0.26	1.67 ± 0.18	0.60 ± 0.23	0.49 ± 0.13	0.76 ± 0.19
$\langle c\rangle$	5.60 ± 0.43	1.85 ± 0.37	0.97 ± 0.18	0.88 ± 0.20	1.17 ± 0.27
$\langle d\rangle$	5.73 ± 0.54	1.57 ± 0.38	1.05 ± 0.28	0.87 ± 0.25	1.14 ± 0.35
$\langle e\rangle$	5.65 ± 0.63	1.83 ± 0.54	1.50 ± 0.41	1.34 ± 0.45	1.77 ± 0.53
$\langle f\rangle$	6.16 ± 0.74	2.03 ± 0.47	1.99 ± 0.75	1.81 ± 0.71	2.34 ± 0.84
$\langle g\rangle$	6.21 ± 0.60	2.19 ± 0.59	2.29 ± 0.76	2.12 ± 0.71	2.62 ± 0.80

[a] The coordinates for classical A- and B-DNA are taken from the fiber diffraction data of Arnott and Hukins (1972). [b] $\bar{a}$ and $\bar{b}$ are the mean structures obtained by averaging the coordinates of the six $\langle a\rangle$ and $\langle b\rangle$ structures, respectively, best fitted to each other.

chemistry and near optimal van der Waals contacts. The latter are particularly important as the NOE distance restraints are strictly limited to interactions between adjacent base pairs. (I.e., unlike in the case of proteins, there are *no* long-range tertiary NOEs in oligonucleotides.)

All the structures satisfy the restraints against which they were calculated within experimental error (Figure 2). Obviously, though, the looser the restraints, the more easily they are satisfied. Hence, the looser the restraints, the smaller the value of E_{NOE} and the rms difference between the calculated and experimental distances.

Structures calculated with a data set x will not satisfy the restraints from a data set with narrower distance limits but will always satisfy the restraints from a data set with larger distance limits (Figure 2). Further, as the restraint limits are widened, so the atomic rms differences between the RD structures within a set increase (Table IV and Figure 3). This is expected as the conformational space consistent with the restraints is increased. Hence, the empirical portion of the total energy function does not affect convergence with respect to either the interproton distances or to structure.

Both the intraresidue and interresidue restraints are important for distinguishing A- and B-DNA. Thus, even for the largest limits used (−1.2/+1.3 Å for $r < 2.5$ Å and −1.3/+1.4Å for $r \geq 2.5$ Å), convergence to B-type structures occurs (Table IV and Figure 3). This is because A-DNA fails to satisfy these

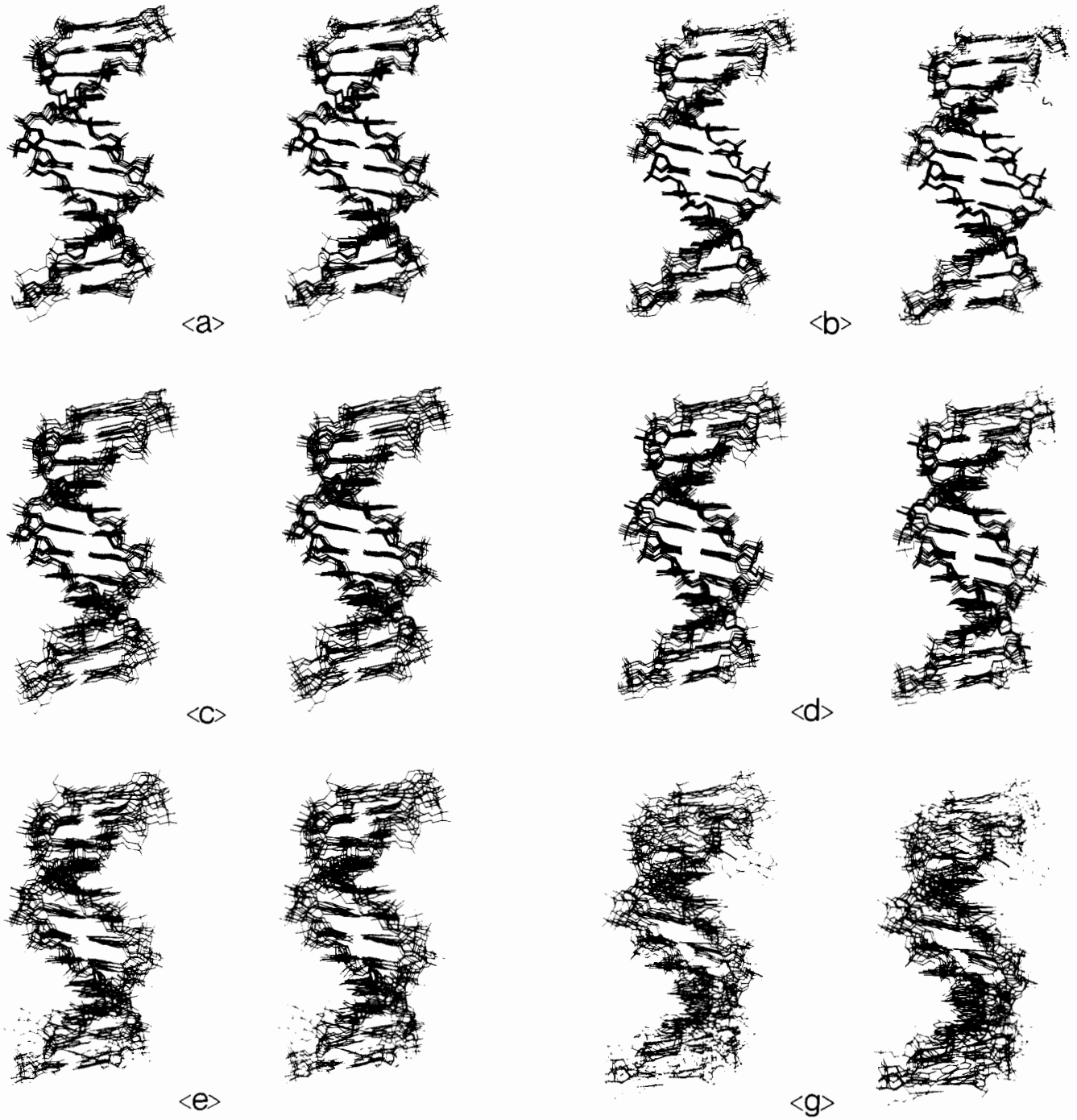

FIGURE 3: Stereoviews of the different RD structure sets.

loose restraints while B-DNA does not.

The *details*, however, of the structures are determined *only* by the interresidue distances, as the intraresidue restraints are satisfied just as well in classical B-DNA as in any of the RD structures, with the exception of the $\langle a \rangle$ set structures where they are satisfied slightly better than by classical B-DNA. (Figure 2).

From the data in Figure 4 it is clear that local structural variations can be well determined up to the *b* restraints set (−0.2/+0.3 Å for $r < 2.5$ Å and −0.3/+0.4 Å for $r \geq 2.5$ Å), as illustrated for the helical parameters and χ glycosidic bond and δ C4′–C3′ torsion angles for residues C3 and A6. Up to the *d* restraints set (−0.4/+0.5 Å for $r < 2.5$ Å and −0.5/+0.6 Å for $r \geq 2.5$ Å) the local structural variations are still discernible, although the spread of the structures becomes appreciably larger, as seen in Figure 3, thereby precluding any detailed interpretation of local conformational parameters. Beyond that, local structural variations cannot be assessed at all. Further, the $\langle a \rangle$ and $\langle b \rangle$ set structures are essentially identical with the structures we previously calculated (Clore et al., 1988) using a biharmonic effective NOE potential. The atomic rms distributions among the $\langle a \rangle$ and $\langle b \rangle$ set structures are 0.47 ± 0.18 and 0.49 ± 0.13 Å, which are very similar to that found for the structures calculated with the biharmonic potential (0.43 ± 0.13 Å). Further, the local structural variations that are illustrated for two selected bases (C3 and A6) in Figure 4 are virtually identical for the *a* and *b* set structures, as well as for those in our previous study. Thus, both the biharmonic potential with upper and lower force constants of 59.6 and 26.5 kcal mol^{-1} Å^{-2} for $r < 2.5$ Å and 26.5 and 14.9 kcal mol^{-1} Å^{-2} for $r \geq 2.5$ Å and the square-well potentials with force constants of 200 kcal mol^{-1} Å^{-2} and error ranges of −0.1/+0.2 or −0.2/+0.3 Å for $r < 2.5$ Å and −0.2/+0.3 or −0.3/+0.4 Å for $2.5 \leq r \leq 5$ Å lead to structures that are

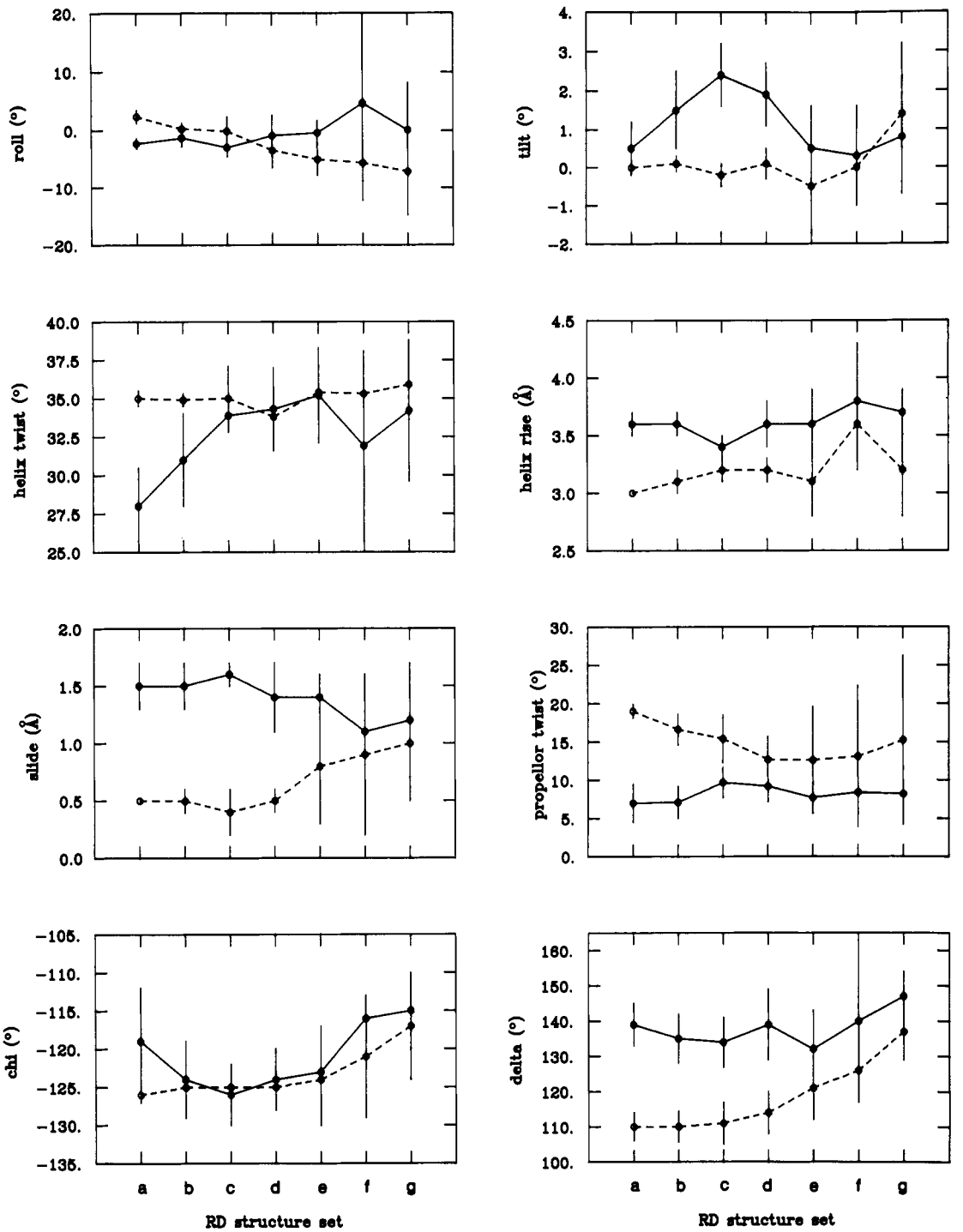

FIGURE 4: Mean values and standard deviations for various helical parameters as well as the χ and δ torsion angles of residues C3 (●—●) and A6 (●---●) for the eight RD structure sets. The vertical bars represent the standard deviations in the values. The helical parameters are calculated by using the program HETRAN (Nilges et al., 1987a), which is a modified version of the programs AHELIX (written by J. Rosenberg), BROLL, and CYLIN (written by R. E. Dickerson).

essentially identical within the precision of the method (i.e., an atomic rms difference of ≤ 1 Å).

Concluding Remarks

The present study shows that the use of restrained molecular dynamics for the structure determination of oligonucleotides on the basis of NMR-derived interproton distance data yields reasonably well defined structures up to error estimates of $\sim 10\%$ for distance restraints up to ~ 4 Å. In most cases, it is easily possible to obtain distance data from NOE measurements within this range of accuracy. Although the driving force for the structural changes that take place during the course of the restrained molecular dynamics calculations lies principally in the interproton distance restraints, it is important in the case of oligonucleotides to use the full empirical energy function to ensure near optimal nonbonded contacts. This seems to be lacking in structures determined by distance geometry methods where only a hard sphere van der Waals repulsion term is used to represent the nonbonded interactions. The effect of the latter appears to be the generation of structures in which the double helix is systematically underwound (Reid, 1987; Nerdal et al., 1988). The probable reason is that errors in the van der Waals repulsion term propagate along the entire structure and lead to obvious structural distortions such as bending. This appears not to be the case with the present protocol of restrained molecular dynamics, which

therefore provides a more reliable method for structure determination of oligonucleotides on the basis of NMR restraints.

ACKNOWLEDGMENTS

We thank Dr. Bernie Brooks for adapting the program X-PLOR for the Star ST-50 array processor.

REFERENCES

Arnott, S., & Hukins, D. W. L. (1972) *Biochem. Biophys. Res. Commun. 47*, 1504–1509.

Behling, R. W., Rao, S. N., Kollman, P., & Kearns, D. R. (1987) *Biochemistry 26*, 4674–4681.

Brooks, B. R., Bruccoleri, R. E., Olafson, B. D., States, D. J., Swaminathan, S., & Karplus, M. (1983) *J. Comput. Chem. 74*, 187–217.

Brünger, A. T. (1988) X-PLOR 1.5 Manual, Yale University, New Haven, CT.

Brünger, A. T., Clore, G. M., Gronenborn, A. M., & Karplus, M. (1986) *Proc. Natl. Acad. Sci. U.S.A. 83*, 3801–3805.

Brünger, A. T., Kuriyan, J., & Karplus, M. (1987) *Science (Washington, D.C.) 235*, 458–460.

Clore, G. M., & Gronenborn, A. M. (1987) *Protein Eng. 1*, 275–288.

Clore, G. M., & Gronenborn, A. M. (1989) *CRC Crit. Rev. Biochem.* (in press).

Clore, G. M., Gronenborn, A. M., Brünger, A. T., & Karplus, M. (1985) *J. Mol. Biol. 186*, 435–455.

Clore, G. M., Brünger, A. T., Karplus, M., & Gronenborn, A. M. (1986a) *J. Mol. Biol. 191*, 523–551.

Clore, G. M., Nilges, M., Sukumaran, D. K., Brünger, A. T., Karplus, M., & Gronenborn, A. M. (1986b) *EMBO J. 5*, 2729–2735.

Clore, G. M., Oschkinat, H., McLaughlin, L. W., Benseler, F., Scalfi Happ, C., Happ, E., & Gronenborn, A. M. (1988) *Biochemistry 27*, 4185–4197.

Gelin, G. R., & Karplus, M. (1975) *Proc. Natl. Acad. Sci. U.S.A. 72*, 2002–2006.

Hare, D. R., & Reid, B. R. (1986) *Biochemistry 25*, 5341–5350.

Hare, D. R., Shapiro, L., & Patel, D. (1986a) *Biochemistry 25*, 7445–7456.

Hare, D. R., Shapiro, L., & Patel, D. (1986b) *Biochemistry 25*, 7456–7464.

Kaptein, R., Zuiderweg, E. R. P., Scheek, R. M., Boelens, R., & van Gunsteren, W. F. (1985) *J. Mol. Biol. 182*, 179–182.

Nerdal, W., Hare, D. R., & Reid, B. R. (1988) *J. Mol. Biol. 201*, 717–739.

Nilges, M., Clore, G. M., Gronenborn, A. M., Brünger, A. T., Karplus, M., & Nilsson, L. (1987a) *Biochemistry 26*, 3718–3733.

Nilges, M., Clore, G. M., Gronenborn, A. M., Piel, N., & McLaughlin, L. W. (1987b) *Biochemistry 26*, 3734–3744.

Nilges, M., Clore, G. M., & Gronenborn, A. M. (1988) *FEBS Lett. 239*, 129–136.

Nilsson, L., & Karplus, M. (1986) *J. Comput. Chem. 7*, 691–716.

Nilsson, L., Clore, G. M., Gronenborn, A. M., Brünger, A. T., & Karplus, M. (1986) *J. Mol. Biol. 188*, 455–475.

Pardi, A., Hare, D. R., & Wang, C. (1988) *Proc. Natl. Acad. Sci. U.S.A. 85*, 8785–8789.

Patel, D. J., Shapiro, L., & Hare, D. R. (1987) *Annu. Rev. Biophys. Biophys. Chem. 16*, 423–454.

Reid, B. R. (1987) *Q. Rev. Biophys. 20*, 1–34.

Rosenberg, J. M., Seeman, N. C., Day, R. O., & Rich, A. (1976) *J. Mol. Biol. 104*, 145–167.

Ryckaert, J. P., Cicotto, G., & Berendsen, H. J. C. (1977) *J. Comput. Phys. 23*, 327–337.

Scalfi Happ, C., Happ, E., Nilges, M., Gronenborn, A. M., & Clore, G. M. (1988) *Biochemistry 27*, 1735–1743.

Seeman, N. C., Rosenberg, J. M., Suddath, F. L., Kim, J. J. P., & Rich, A. (1976) *J. Mol. Biol. 104*, 109–144.

Tidor, B., Irikura, K., Brooks, B. R., & Karplus, M. (1983) *J. Biomol. Struct. Dyn. 1*, 231–252.

Verlet, L. (1967) *Phys. Rev. 159*, 98–105.

Wüthrich, K. (1986) *NMR of Proteins and Nucleic Acids*, Wiley, New York.

Wüthrich, K. (1989) *Science (Washington, D.C.) 243*, 45–50.